



Copyright Notice

This paper was published in *Optics Express* and is made available as an electronic reprint with the permission of OSA. The paper can be found at the following URL on the OSA website: <http://dx.doi.org/10.1364/OE.19.012093>. Systematic or multiple reproduction or distribution to multiple locations via electronic or other means is prohibited and is subject to penalties under law.

(Article begins on next page)

Optical response of supported gold nanodisks

A. Mendoza-Galván,^{1,2,*} K. Järrendahl,² A. Dmitriev,³
T. Pakizeh,⁴ M. Käll,³ and H. Arwin^{2,5}

¹*Cinvestav-IPN, Unidad Querétaro, Libramiento Norponiente 2000, 76230 Querétaro, Mexico*

²*Laboratory of Applied Optics, Department of Physics, Chemistry and Biology, Linköping University, SE-581 83 Linköping, Sweden*

³*Department of Applied Physics, Chalmers University of Technology, SE-412 96 Göteborg, Sweden*

⁴*Faculty of Electrical and Computer Engineering, K. N. Toosi University of Technology, Tehran 16314, Iran*

⁵*hansa@ifm.liu.se*

**amendoza@gro.cinvestav.mx*

Abstract: It is shown that the ellipsometric spectra of short range ordered planar arrays of gold nanodisks supported on glass substrates can be described by modeling the nanostructured arrays as uniaxial homogeneous layers with dielectric functions of the Lorentz type. However, appreciable deviations from experimental data are observed in calculated spectra of irradiance measurements. A qualitative and quantitative description of all measured spectra is obtained with a uniaxial effective medium dielectric function in which the nanodisks are modeled as oblate spheroids. Dynamic depolarization factors in the long-wavelength approximation and interaction with the substrate are considered. Similar results are obtained calculating the optical spectra using the island-film theory. Nevertheless, a small in-plane anisotropy and quadrupolar coupling effects reveal a very complex optical response of the nanostructured arrays.

©2011 Optical Society of America

OCIS codes: (240.2130) Ellipsometry and polarimetry; (240.6680) Surface plasmons; (160.1190) Anisotropic optical materials; (160.1245) Artificially engineered materials; (160.4760) Optical properties.

References and links

1. C. F. Bohren and D. R. Huffman, *Absorption and Scattering of Light by Small Particles* (John Wiley & Sons, 1983).
2. N. V. Voshchinnikov and V. G. Farafonov, "Optical properties of spheroidal particles," *Astrophys. Space Sci.* **204**(1), 19–86 (1993).
3. M. E. Stewart, C. R. Anderton, L. B. Thompson, J. Maria, S. K. Gray, J. A. Rogers, and R. G. Nuzzo, "Nanostructured plasmonic sensors," *Chem. Rev.* **108**(2), 494–521 (2008).
4. N. G. Khlebtsov and L. A. Dykman, "Optical properties and biomedical applications of plasmonic nanoparticles," *J. Quant. Spectrosc. Radiat. Transf.* **111**(1), 1–35 (2010).
5. K. L. Kelly, E. Coronado, L. L. Zhao, and G. C. Schatz, "The optical properties of metal nanoparticles: the influence of size, shape, and dielectric environment," *J. Phys. Chem. B* **107**(3), 668–677 (2003).
6. V. K. S. Hsiao, Y. B. Zheng, B. K. Juluri, and T. J. Huang, "Light-driven plasmonic switches based on Au nanodisk arrays and photoresponsive liquid crystals," *Adv. Mater. (Deerfield Beach Fla.)* **20**(18), 3528–3532 (2008).
7. M. Svedendahl, S. Chen, A. Dmitriev, and M. Käll, "Refractometric sensing using propagating versus localized surface plasmons: a direct comparison," *Nano Lett.* **9**(12), 4428–4433 (2009).
8. H. Fredriksson, Y. Alaverdyan, A. Dmitriev, C. Langhammer, D. S. Sutherland, M. Zäch, and B. Kasemo, "Hole-mask colloidal lithography," *Adv. Mater. (Deerfield Beach Fla.)* **19**(23), 4297–4302 (2007).
9. T. Pakizeh, M. S. Abrishamian, N. Granpayeh, A. Dmitriev, and M. Käll, "Magnetic-field enhancement in gold nanosandwiches," *Opt. Express* **14**(18), 8240–8246 (2006).
10. A. Dmitriev, T. Pakizeh, M. Käll, and D. S. Sutherland, "Gold-silica-gold nanosandwiches: tunable bimodal plasmonic resonators," *Small* **3**(2), 294–299 (2007).
11. T. Pakizeh, A. Dmitriev, M. S. Abrishamian, N. Granpayeh, and M. Käll, "Structural asymmetry and induced optical magnetism in plasmonic nanosandwiches," *J. Opt. Soc. Am. B* **25**(4), 659–667 (2008).
12. T. Pakizeh, C. Langhammer, I. Zorić, P. Apell, and M. Käll, "Intrinsic Fano interference of localized plasmons in Pd nanoparticles," *Nano Lett.* **9**(2), 882–886 (2009).
13. B. Sepúlveda, J. B. González-Díaz, A. García-Martín, L. M. Lechuga, and G. Armelles, "Plasmon-induced magneto-optical activity in nanosized gold disks," *Phys. Rev. Lett.* **104**(14), 147401 (2010).
14. P. Hanarp, M. Käll, and D. S. Sutherland, "Optical properties of short range ordered arrays of nanometer gold disks prepared by colloidal lithography," *J. Phys. Chem. B* **107**(24), 5768–5772 (2003).

15. C. Langhammer, Z. Yuan, I. Zorić, and B. Kasemo, "Plasmonic properties of supported Pt and Pd nanostructures," *Nano Lett.* **6**(4), 833–838 (2006).
16. C. Langhammer, B. Kasemo, and I. Zorić, "Absorption and scattering of light by Pt, Pd, Ag, and Au nanodisks: absolute cross sections and branching ratios," *J. Chem. Phys.* **126**(19), 194702 (2007).
17. Y. B. Zheng, B. Kiraly, S. Cheunkar, T. J. Huang, and P. S. Weiss, "Incident-angle-modulated molecular plasmonic switches: a case of weak exciton-plasmon coupling," *Nano Lett.* **11**(5), 2061–2065 (2011).
18. Y. B. Zheng, B. K. Juluri, L. Lin Jensen, D. Ahmed, M. Lu, L. Jensen, and T. J. Huang, "Dynamical tuning of plasmon-exciton coupling in arrays of nanodisk-J-aggregate complexes," *Adv. Mater. (Deerfield Beach Fla.)* **22**(32), 3603–3607 (2010).
19. T. Yang and K. B. Crozier, "Surface plasmon coupling in periodic metallic nanoparticle structures: a semi-analytical model," *Opt. Express* **16**(17), 13070–13079 (2008).
20. T. Yang and K. B. Crozier, "Dispersion and extinction of surface plasmons in an array of gold nanoparticle chains: influence of the air/glass interface," *Opt. Express* **16**(12), 8570–8580 (2008).
21. K. B. Crozier, E. Togan, E. Simsek, and T. Yang, "Experimental measurement of the dispersion relations of the surface plasmon modes of metal nanoparticle chains," *Opt. Express* **15**(26), 17482–17493 (2007).
22. E. Ringe, J. M. McMahon, K. Sohn, C. Cobley, Y. Xia, J. Huang, G. C. Schatz, L. D. Marks, and R. P. Van Duyne, "Unraveling the effects of size, composition, and substrate on the localized surface plasmon resonance frequencies of gold and silver nanocubes: a systematic single-particle approach," *J. Phys. Chem. C* **114**(29), 12511–12516 (2010).
23. C. P. Burrows and W. L. Barnes, "Large spectral extinction due to overlap of dipolar and quadrupolar plasmonic modes of metallic nanoparticles in arrays," *Opt. Express* **18**(3), 3187–3198 (2010).
24. S. Berthier, "Anisotropic effective medium theories," *J. Phys. I* **4**(2), 303–318 (1994).
25. T. Yamaguchi, S. Yoshida, and A. Kinbara, "Optical effect of the substrate on the anomalous absorption of aggregated silver films," *Thin Solid Films* **21**(1), 173–187 (1974).
26. V. A. Fedotov, V. I. Emel'yanov, K. F. MacDonald, and N. I. Zheludev, "Optical properties of closely packed nanoparticle films: spheroids and nanoshells," *J. Opt. A, Pure Appl. Opt.* **6**(2), 155–160 (2004).
27. D. Bedeaux and J. Vlieger, *Optical Properties of Surfaces* (Imperial College Press, 2001).
28. R. Lazzari and I. Simonsen, "GRANFILM: a software for calculating thin-layer dielectric properties and Fresnel coefficients," *Thin Solid Films* **419**(1-2), 124–136 (2002).
29. H. Wormeester, E. S. Kooij, A. Mewe, S. Rekveld, and B. Poelsema, "Ellipsometric characterisation of heterogeneous 2D layers," *Thin Solid Films* **455–456**, 323–334 (2004).
30. H. Wormeester, A.-I. Henry, E. S. Kooij, B. Poelsema, and M. P. Pileni, "Ellipsometric identification of collective optical properties of silver nanocrystal arrays," *J. Chem. Phys.* **124**(20), 204713 (2006).
31. J. M. Flores-Camacho, L. D. Sun, N. Saucedo-Zeni, G. Weidlinger, M. Hohage, and P. Zeppenfeld, "Optical anisotropies of metal clusters supported on a birefringent substrate," *Phys. Rev. B* **78**(7), 075416 (2008).
32. M. Losurdo, M. Bergmair, G. Bruno, D. Cattelan, C. Cobet, A. Martino, K. Fleischer, Z. Dohcevic-Mitrovic, N. Esser, M. Galliet, R. Gajic, D. Hemzal, K. Hingerl, J. Humlicek, R. Ossikovski, Z. V. Popovic, and O. Saxl, "Spectroscopic ellipsometry and polarimetry for materials and systems analysis at the nanometer scale: state-of-the-art, potential, and perspectives," *J. Nanopart. Res.* **11**(7), 1521–1554 (2009).
33. K. Johansen, H. Arwin, I. Lundström, and B. Liedberg, "Imaging surface plasmon resonance sensor based on multiple wavelengths: sensitivity considerations," *Rev. Sci. Instrum.* **71**(9), 3530–3538 (2000).
34. R. M. A. Azzam and N. M. Bashara, *Ellipsometry and Polarized Light* (North Holland, 1977).
35. G. Xu, Y. Chen, M. Tazawa, and P. Jin, "Influence of dielectric properties of a substrate upon plasmon resonance spectrum of supported Ag nanoparticles," *Appl. Phys. Lett.* **88**(4), 043114 (2006).
36. C. A. Foss, G. L. Hornyak, J. A. Stockert, and C. R. Martin, "Template-synthesized nanoscopic gold particles: optical spectra and the effects of particle size and shape," *J. Phys. Chem.* **98**(11), 2963–2971 (1994).
37. M. Meier and A. Wokaun, "Enhanced fields on large metal particles: dynamic depolarization," *Opt. Lett.* **8**(11), 581–583 (1983).
38. A. Moroz, "Depolarization field of spheroidal particles," *J. Opt. Soc. Am. B* **26**(3), 517–527 (2009).
39. R. Esteban, R. Vogelgesang, J. Dorfmueller, A. Dmitriev, C. Rockstuhl, C. Etrich, and K. Kern, "Direct near-field optical imaging of higher order plasmonic resonances," *Nano Lett.* **8**(10), 3155–3159 (2008).
40. R. Boyack and E. C. Le Ru, "Investigation of particle shape and size effects in SERS using T-matrix calculations," *Phys. Chem. Chem. Phys.* **11**(34), 7398–7405 (2009).
41. I. O. Sosa, C. Noguez, and R. G. Barrera, "Optical properties of metal nanoparticles with arbitrary shapes," *J. Phys. Chem. B* **107**(26), 6269–6275 (2003).
42. C. E. Román-Velázquez, C. Noguez, and R. G. Barrera, "Substrate effects on the optical properties of spheroidal nanoparticles," *Phys. Rev. B* **61**(15), 10427–10436 (2000).
43. R. Lazzari, S. Roux, I. Simonsen, J. Jupille, D. Bedeaux, and J. Vlieger, "Multipolar plasmon resonances in supported silver particles: the case of Ag/ α -Al₂O₃ (0001)," *Phys. Rev. B* **65**(23), 235424 (2002).
44. Y. Ekinci, A. Christ, M. Agio, O. J. F. Martin, H. H. Solak, and J. F. Löffler, "Electric and magnetic resonances in arrays of coupled gold nanoparticle in-tandem pairs," *Opt. Express* **16**(17), 13287–13295 (2008).

1. Introduction

The optical properties of metallic nanoparticles have been of interest for many years and the scattering of electromagnetic waves by spheres and spheroids has been rigorously calculated before [1,2]. One of the most interesting properties resulting from the interaction between

electromagnetic waves and metallic nanoparticles is the excitation of collective oscillations of the conduction electrons, i.e. localized surface plasmon resonances (LSPRs). The LSPRs dependence on the size and shape of nanoparticles and the surrounding environment has attracted much attention due to potential applications in different devices [3–7]. Of special interest are nanostructured arrays supported on a substrate as those fabricated by hole-mask colloidal lithography [8]. This technique allows control of shapes and sizes in the fabrication of an ample variety of nanostructures including disks, ellipses, cones, binary nanoparticles [8] as well composite nanostructures like metal-dielectric-metal structures [9–11]. Besides the LSPR observed in metallic nanostructures, the scientific literature reports on other interesting phenomena like optical magnetism in nanosandwiches [9–11], intrinsic Fano interference of localized plasmons in Pd nanoparticles [12], and plasmon induced magneto-optical activity [13].

Although there are many reports on the optical properties of metallic nanoparticles supported on a substrate, there are still some remaining gaps that deserve attention. First, for large nanoparticles (length scales of several tens or a few hundreds of nm) many of the studies are performed by only analyzing the extinction spectra obtained from transmittance measurements at normal incidence. In particular, the LSPRs of Au, Ag, Pt, and Pd nanodisks short-range ordered arrays have been previously studied by modeling the nanodisks as oblate spheroids in the modified long wavelength approximation [14–16]. However, under normal incidence the analysis is limited to only the component (in-plane) of the polarizability tensor parallel to the substrate. Furthermore, the effect of the substrate is taken into account by assuming that the spheroids are embedded in an effective medium of refractive index given by the average between the ambient and substrate. On the other hand, both experimental and theoretical optical studies of periodic gold nanoparticle arrays (one- and two-dimensional) have been performed at oblique incidence [17–21]. Therefore, appropriate modeling of optical measurements at oblique incidence is required to retrieve the components of the polarizability tensor. Certainly, electrodynamics calculations are able to extract optical information but often with high computational costs [5,17–23].

The simplest model to describe the optical properties of nanostructured arrays supported on a substrate is a homogeneous anisotropic layer. In this case, the components of the dielectric function tensor can be modeled with Lorentz harmonic-type oscillators or anisotropic effective medium theories [24–26]. For small metallic nanoparticles (length scales < 10 nm) supported on a substrate, in the 2D-effective medium theory of Yamaguchi *et al* [25] and its improved version [26], the interaction between neighboring particles and with the substrate are taken into account in the dipole approximation. On the other hand, higher-order multipole interactions were extensively investigated by Bedeaux and Vlieger leading to the formulation of the island-film theory [27]. This theory is based on the notion of excess quantities and surface susceptibilities providing modified Fresnel coefficients that have successfully explained the optical response of small metallic nanoparticles on a surface [28–31]. At first-order two surface susceptibilities are required: one parallel (γ) and the other perpendicular (β) to the substrate. For non-interacting islands (low coverage), γ and β depend on geometrical details of the islands and the effect of the substrate is taken into account by the charge image technique. As noted above, the 2D-effective medium theory and the island-film theory have not been explored to describe the optical properties of large nanoparticles yet.

Spectroscopic ellipsometry is a well established optical technique for characterization of surfaces, interfaces, and thin films. Recently, its potential use at the nanometer scale has been reviewed [32]. In this work, we have investigated the optical response of gold nanodisks arrays by spectroscopic ellipsometry and irradiance measurements at oblique and normal incidence. Thus, both, the in-plane and out-of-plane components are probed. The data are analyzed using two approaches: *i*) by modeling the nanostructure with a homogenous uniaxial layer with an effective dielectric function of either the Lorentz type (Sec. 3.1) or with a modified Yamaguchi effective medium expression that includes dynamic depolarization factors (Sec. 3.2). *ii*) In the second approach, the island-film theory is applied by modeling the in-plane polarizability in the modified long-wavelength approximation (Sec. 3.3). The

possible origins of the small in-plane anisotropy are discussed in Sec. 3.4. Finally, in Sec. 3.5 the excitation of a quadrupolar mode at larger angles of incidence is briefly discussed.

2. Experimental

Gold nanostructured arrays were fabricated on glass substrates by hole-mask colloidal lithography [8]. The investigated samples are 40 nm thick Au nanodisks as well as 20 nm thick Au nanodisks covered with a 20 nm thick SiO₂ layer. In both cases, the nanodisks are nearly circular with an average diameter of 170 nm as represented in Figs. 1(a) and 1(b). One of the Au nanodisks was capped with a SiO₂ layer in order to investigate the effect of partial embedding on the optical properties of metallic nanoparticles. Also, this structure is part of composite structures like Au-SiO₂-Au nanosandwiches which have shown very interesting optical properties [9–11]. Details of thickness and diameter control during fabrication of Au nanodisks can be found elsewhere [7,10,11,14].

Spectroscopic ellipsometry (SE) measurements were performed in the 300-1300 nm wavelength range using a variable angle spectroscopic ellipsometer (VASE) of rotating analyzer type equipped with an auto-retarder (J. A. Woollam Co., Inc.). Reflectance spectra were measured for polarizations parallel and perpendicular to the plane of incidence. For measurements in reflection mode the back side of the substrate was roughened and the angles of incidence were between 50° and 70°. Also, transmission ellipsometry and irradiance transmittance (p-polarized) spectra at normal incidence were acquired. The refractive index of the glass substrate was determined from ellipsometric data and then its extinction coefficient was obtained by a point-by-point fitting of transmittance spectra at normal incidence. The complex dielectric function of gold was taken from VASE measurements of a homogeneous gold film [33].

SE measures the change in the polarization state that incident polarized light experiences due to interaction with a sample. In reflection (transmission) mode the change is described by the complex-valued ratio ρ_r (ρ_t) between the reflection (transmission) coefficients for light polarized parallel r_p (t_p) and perpendicular r_s (t_s) to the plane of incidence [34],

$$\rho_r = \frac{r_p}{r_s} = \tan \Psi_r \exp(i\Delta_r), \quad \rho_t = \frac{t_p}{t_s} = \tan \Psi_t \exp(i\Delta_t), \quad (1)$$

where ρ_r (ρ_t) is expressed in terms of the two ellipsometric angles Ψ and Δ which depend on the microstructure and optical properties of the constituents of the sample. Thus, the construction of an optical model for the reflection (transmission) coefficients r_p (t_p) and r_s (t_s) allows the determination of parameters like film thicknesses, complex dielectric functions, volume fractions, etc., of a multilayer model representing the sample. Those parameters are obtained in a fitting procedure minimizing the mean square error (MSE) between the model and experimental data,

$$MSE = \frac{1}{2N - M} \sum_{i=1}^N \left[\left(\frac{\Psi_i^{\text{mod}} - \Psi_i^{\text{exp}}}{\sigma_{\Psi_i}^{\text{exp}}} \right)^2 + \left(\frac{\Delta_i^{\text{mod}} - \Delta_i^{\text{exp}}}{\sigma_{\Delta_i}^{\text{exp}}} \right)^2 \right], \quad (2)$$

where N is the number of measured Ψ - Δ pairs, M the total number of fit parameters, and σ^{exp} are the standard deviations of the measurements. The superscripts *mod* and *exp* indicate model-calculated and experimental data, respectively. The non-linear regression algorithm also provides 90% confidence limits of the fitted parameters.

3. Results and discussion

3.1 Homogeneous uniaxial layer approach

Figure 1 shows a schematic representation of the investigated samples: (a) 40 nm thick gold nanodisks and (b) SiO₂-capped 20 nm thick gold nanodisks. In both cases the nanodisks are deposited on a glass substrate with dielectric function ϵ_s in an ambient with dielectric function

ϵ_a . As a first approach, the optical response of these nanostructured arrays will be described as a continuous layer of thickness d and with a dielectric tensor $\text{diag}(\epsilon_x, \epsilon_y, \epsilon_z)$, Fig. 1(c). The origin of this anisotropy is clear from the structure of the arrays because applying an electric field either parallel or perpendicular to the sample surface, the optical response of the nanostructured array will be different. Furthermore, the nearly circular shape of the nanodisks allows the definition of the in-plane ($\epsilon_x = \epsilon_y = \epsilon_{//}$) and out-of-plane ($\epsilon_z = \epsilon_{\perp}$) components of a homogeneous uniaxial layer.

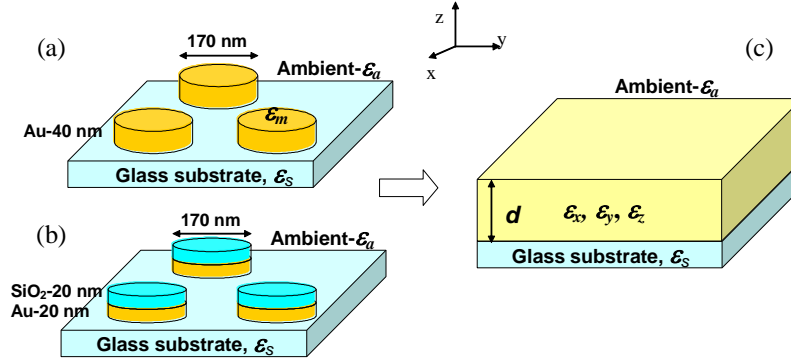


Fig. 1. Schematic representation of the investigated nanostructures: (a) Gold nanodisks, (b) Silica-covered gold nanodisks, (c) Anisotropic homogeneous layer with thickness d and effective dielectric function ϵ .

Figures 2(a) and 2(b) show the experimental VASE data and the best fit using the homogenous uniaxial layer model for the silica-capped Au nanodisks array. The in-plane $\epsilon_{//}$ and out-of-plane ϵ_{\perp} components are represented with a single Lorentz oscillator according to the expression,

$$\epsilon_{L,(\parallel, \perp)}(E) = \epsilon_{\infty(\parallel, \perp)} + \frac{A_{(\parallel, \perp)} B_{(\parallel, \perp)} E_{c,(\parallel, \perp)}}{E_{c,(\parallel, \perp)}^2 - E^2 + i B_{(\parallel, \perp)} E}. \quad (3)$$

where E is the photon energy, ϵ_{∞} is the high frequency dielectric constant; A , B , and E_c are the oscillator amplitude, broadening, and central energy, respectively. The fitting was performed with the WVASE32 software (J. A. Woollam Co., Inc.). For the fitting, the layer thickness was fixed to $d = 20$ nm, corresponding to the thickness of the Au-nanodisks. Otherwise, leaving d as a fitting parameter, its correlation with $A_{//}$, $\epsilon_{\infty//}$, and $\epsilon_{\infty\perp}$ became very large. Thus, the fitting parameters are only those of Eq. (3). The obtained values and confidence limits as well as the MSE given by Eq. (2) are presented in Table 1. The components of the complex dielectric tensor $\epsilon_{L,//}$ and $\epsilon_{L,\perp}$ are shown in Fig. 2(c) where clearly a strong anisotropy of the nanostructured array is observed. It should be mentioned that if the total thickness of the nanostructure is considered in the fitting, i.e. $d = d_{\text{silica}} + d_{\text{Au}} = 40$ nm, the result is identical to that in Figs. 2(a) and 2(b) but with parameters $A_{//} = 1.11$, $\epsilon_{\infty//} = 0.74$, $A_{\perp} = 0.03$, and $\epsilon_{\infty\perp} = 0.94$ whereas the broadening and central energy remained the same as in Table 1. Also, similar results were obtained considering either the weight thicknesses of about 2 nm or any other effective thickness ranging between 2 and 40 nm. Furthermore, it has been previously reported that for 10 nm thick and 110 nm in diameter gold nanodisks array the location of the plasmon resonance is not affected by capping with 20 nm of silica [10].

At this point, it seems natural to conclude that the optical response of the nanodisks array can be given in terms of the homogeneous uniaxial layer 20 nm thick with effective dielectric functions $\epsilon_{L,//}$ and $\epsilon_{L,\perp}$ of Fig. 2(c). However, in order to investigate whether or not the model truly describes the optical response of the nanostructured array, a comparison should be established with independent measurements as is done in Figs. 2(d)–2(f). Figure 2(d) shows

that the experimental spectra of oblique p-polarized reflectance (R_p) are well described by the model-calculations. For s-polarization (R_s), presented in Fig. 2(e), the calculated data fairly describe the plasmon resonance but appreciably differences are observed at short wavelengths. In addition, as the angle of incidence increases the experimental data of R_s show a shoulder at about 640 nm and also noticed in the R_p spectrum at 70°. The origin of this feature (Q) indicated by the arrows in Figs. 2(d) and 2(e) is discussed in Sec. 3.5. Another discrepancy is noticed in irradiance transmittance (T) at normal incidence (Fig. 2(f)). In this case, the plasmon resonance obtained from the model-calculations is broader and shifted to longer wavelengths compared to the experimental data.

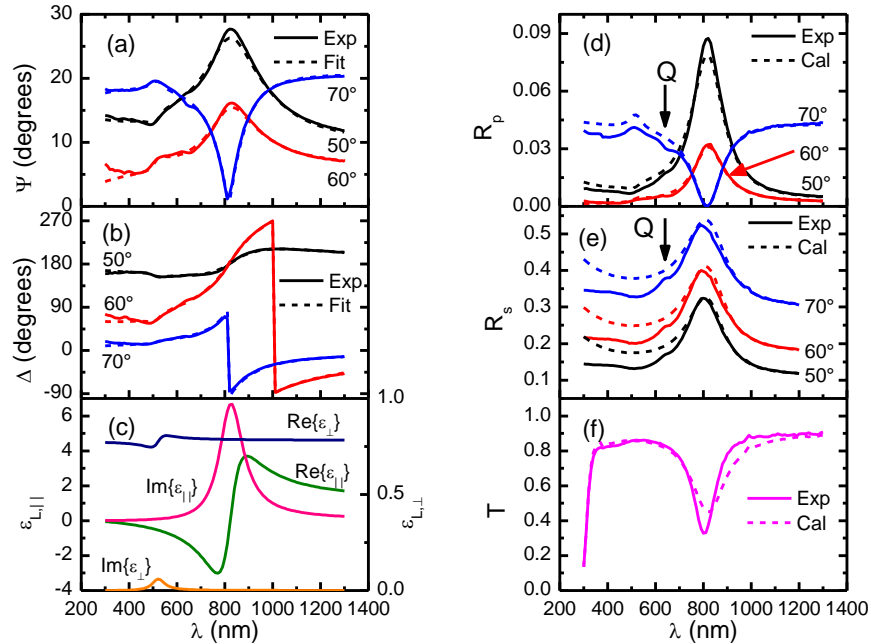


Fig. 2. Experimental and best fit ellipsometric spectra of Ψ (a) and Δ (b) for a silica capped gold nanodisks array with thickness 20 nm using the Lorentz oscillator dielectric tensor components shown in (c). Comparison between experimental and model-calculated data for: (d) oblique reflectance of p-polarized and (e) s-polarized light, as well as (f) normal incidence transmittance.

VASE data for the array with 40 nm thick gold nanodisks are shown in Figs. 3(a) and 3(b). Once again, an excellent fit was obtained using the nanodisks thickness as the layer thickness. Fitting parameters and confidence limits are presented in Table 1 and the effective dielectric function tensor components obtained are shown in Fig. 3(c). As can be seen in Figs. 3(d)–3(f), major discrepancies are obtained between the experimental and model-calculated spectra of R_p , R_s , and T for this thicker nanodisks array. In Figs. 3(d) and 3(e) also is observed a feature at about 600 nm (Q) in the experimental R_p spectrum at 70° and in the three R_s spectra. In summary, the successful description of the SE data modeling the nanostructured arrays as a homogeneous uniaxial layer does not assure that the dielectric tensor of Lorentz-type obtained represents reliable materials properties. Therefore, other approaches should be used as will be shown below.

Table 1. Parameters of the Lorentz Effective Dielectric Tensor Function Representing the Supported Nanodisks

Parameter	Nanodisks 20 nm thick		Nanodisks 40 nm thick	
	$\epsilon_{ }$	ϵ_{\perp}	$\epsilon_{ }$	ϵ_{\perp}
ϵ_{∞}	0.10 ± 0.03	0.78 ± 0.006	0.24 ± 0.02	0.79 ± 0.004
A	2.23 ± 0.007	0.04 ± 0.003	1.55 ± 0.007	0.06 ± 0.002
B (eV)	0.22 ± 0.001	0.29 ± 0.03	0.36 ± 0.002	0.32 ± 0.011
E_c (eV)	1.51 ± 0.001	2.38 ± 0.008	1.69 ± 0.001	2.42 ± 0.004
λ_c (nm) ^a	821	521	733	512
MSE	2.5		1.99	

^aWavelength of oscillator central energy: λ_c (nm) = $1239.8/E_c$ (eV).

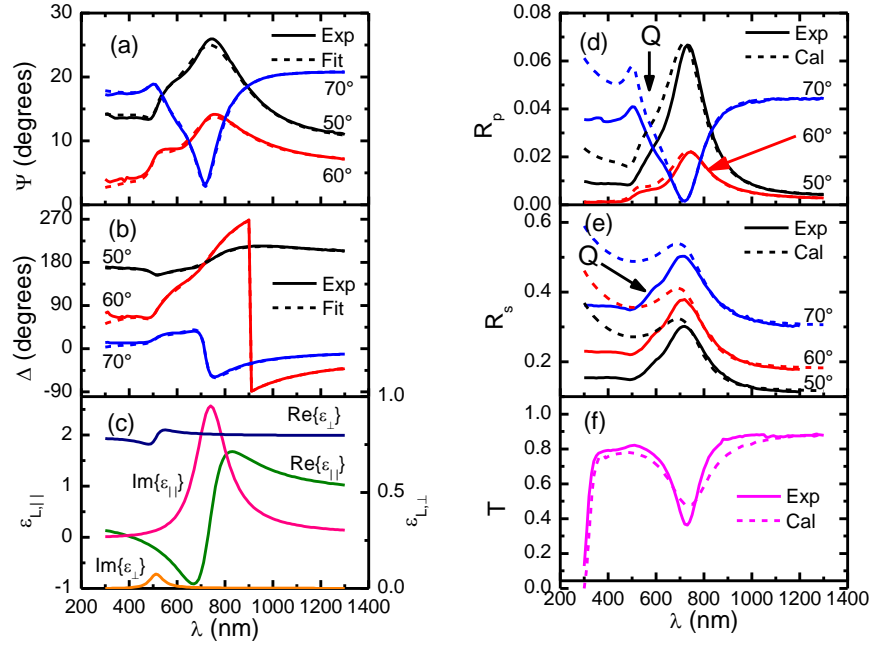


Fig. 3. Experimental and best fit ellipsometric spectra of Ψ (a) and Δ (b) for a 40 nm thick gold nanodisks array using the Lorentz oscillator dielectric response tensor components shown in (c). Comparison between experimental and model-calculated data for: (d) oblique reflectance of p-polarized and (e) s-polarized light, as well as (f) normal incidence transmittance.

3.2 Dynamic Yamaguchi approach

The homogenization procedure depicted in Fig. 1 within the Yamaguchi effective medium theory lead to effective dielectric function components $\epsilon_{Y,||}$ and $\epsilon_{Y,\perp}$ given by [25],

$$\epsilon_{Y,||} = \epsilon_a \left[1 + q \frac{\epsilon_m - \epsilon_a}{\epsilon_a + F_{||}(\epsilon_m - \epsilon_a)} \right], \quad (4)$$

and,

$$\epsilon_{Y,\perp} = \epsilon_a \left[1 - q \frac{\epsilon_m - \epsilon_a}{\epsilon_a + F_{\perp}(\epsilon_m - \epsilon_a)} \right]^{-1}, \quad (5)$$

where q is the volume fraction occupied by the nanodisks, F_{\parallel} and F_{\perp} are effective depolarization factors, including the dipole interaction between particles and with the substrate. Equations (4) and (5) are applicable for very small particles compared with the wavelength. Since we are dealing with non-interacting nanodisks, F_{\parallel} and F_{\perp} will depend only on their shape and interaction with the substrate. In their original work, Yamaguchi et al use a point dipole approximation to account for interaction of spherical (or near spherical) particles with the substrate [25]. These assumptions impose some limitations to the model which was improved by Fedotov et al by considering the exact local fields of spheroidal particles [26]. Furthermore, dynamic depolarization and radiation damping become important for the in-plane component due to the relative large diameter of the nanodisks. The nanodisks are thus modeled as oblate spheroids with the major (minor) semi-axis $a(c)$ parallel (perpendicular) to the substrate. We introduce the *dynamic depolarization factor* $F_{\parallel,d}$ for the in-plane component as,

$$F_{\parallel,d} = l_{\parallel} - \varepsilon_a \frac{\varepsilon_a - \varepsilon_s}{\varepsilon_a + \varepsilon_s} \frac{e(1+e^2)}{2} \left\{ \frac{2e}{1+4e^2} - \arctan \frac{1}{2e} \right\} - \frac{k^2 ac}{3} - \frac{2ik^3 a^2 c}{9}, \quad (6)$$

whereas the out-of-plane depolarization factor is,

$$F_{\perp} = l_{\perp} - \varepsilon_a \frac{\varepsilon_a - \varepsilon_s}{\varepsilon_a + \varepsilon_s} e(1+e^2) \left\{ \frac{2e}{1+4e^2} - \arctan \frac{1}{2e} \right\}, \quad (7)$$

where $l_{\perp} = (1 + e^2)(1 - e \arctan e^{-1})$ and $l_{\parallel} = (1 - l_{\perp})/2$ are the depolarization factors in the electrostatic limit being $e = ((a/c)^2 - 1)^{-1/2}$ [27]. The second term in Eqs. (6) and (7) accounts for the interaction with the substrate according to Eq. (28) in [26] and represents a modification of the Yamaguchi expression. The third and fourth terms of Eq. (6) correspond to dynamic depolarization and radiation damping, respectively, where $k = 2\pi/\lambda$ is the wave number of the incident light with wavelength λ . In other works, these terms were included in a dynamic Maxwell-Garnett expression and were written as $k^2 a^2/3$ and $2ik^3 a^3/9$, respectively, leading to only qualitative agreement with measurements [35,36]. This is because those terms originally were derived from volume integrals on a sphere [37]. In the case of spheroids those integrals lead to the first, third, and fourth terms in Eq. (6) up to a dynamic geometrical factor multiplying the dynamic depolarization ($\sim k^2$) term [38]. However, it was shown that this kind of factor, which depends on the aspect ratio, produces a considerable red-shift larger than T-matrix calculations [38] and herein is taken as the unity. Therefore, the dielectric tensor of non interacting nanodisks is represented by a *dynamic modified Yamaguchi* expression $\varepsilon_{\text{DMY},\parallel}$ for the in-plane component, Eqs. (4) and (6), whereas a *modified Yamaguchi* expression $\varepsilon_{\text{MY},\perp}$, Eqs. (5) and (7), is used for the out-of-plane component.

Figure 4 shows a comparison between the experimental and calculated spectra for the silica-capped Au nanodisks, schematically shown in Fig. 1(b). For that, Fresnel coefficients of an air-uniaxial film-substrate system [34] were used with dielectric functions components given by Eqs. (4)–(7). The calculations were performed with a FORTRAN code using the parameters: $a = 85$ nm, $c = 10$ nm, $q = 0.065$ and film thickness $d = 20$ nm. In Fig. 4 it can be observed that this model gives a better description of all measured spectra than by using Lorentz expressions shown in Fig. 2. The quantitative agreement seen in Fig. 4 supports the use of Eq. (6) for the description of the LSPR in spheroidal particles. In Fig. 4(f) the transmittance spectrum neglecting the nanodisks-substrate interaction (second term in Eq. (6)) is also included which clearly shows that the LSRP then becomes weaker and blue-shifted. This is explained when considering that according to Eq. (4) the resonance is located at wavelengths where $\text{Re}\{\varepsilon_m\} = (1 - 1/F_{\parallel})\varepsilon_a$ and as the interaction with the substrate decreases F_{\parallel} this condition is fulfilled at longer wavelengths. Capping the Au nanodisks with the SiO_2 layer has not effect on the LSPR because $\varepsilon_a = 1$ in Eq. (4). Although a very good description of the optical spectra is seen in Fig. 4, some differences can be noticed in the spectral location of the extremes in R_p and R_s spectra, Figs. 4(d) and 4(e). The latter were obtained from derivative

spectra of experimental (calculated) data at 817 (810), 822 (815) and 814 (805) nm for R_p ; whereas for R_s the values are 799 (806), 794 (806), and 792 (806) nm for the angles of incidence 50, 60 and 70°, respectively. This different response to p- or s-polarized light is indicative of some in-plane anisotropy as discussed below.

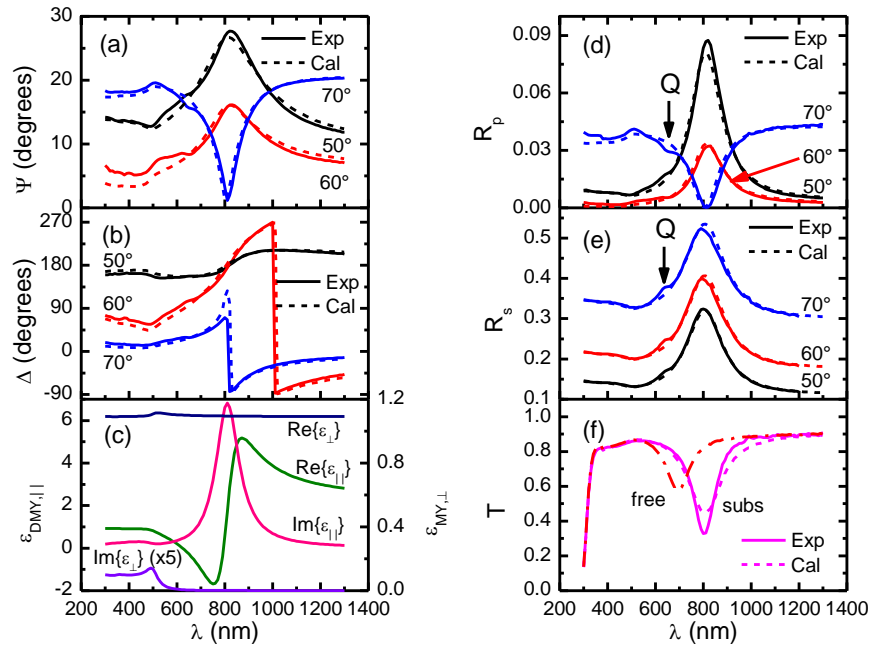


Fig. 4. Experimental and calculated spectra for silica-capped gold nanodisks array 20 nm thick using the dynamic Yamaguchi effective dielectric response assuming gold spheroids: (a) Ψ , (b) Δ , (c) effective dielectric function tensor components, (d) reflectance of p-polarized and (e) s-polarized light, as well as (f) normal incidence transmittance (subs). In (f) also the spectrum for spheroids non interacting with the substrate (free) is included.

Figure 5 shows a comparison of experimental and calculated spectra using Eqs. (4)–(7) for the dielectric function of gold nanodisks array with thickness 40 nm. The parameters used in the calculations were $a = 88$ nm, $c = 19$ nm, $q = 0.065$ and film thickness $d = 38$ nm. Clearly in Figs. 4 and 5 the description of the experimental T , R_p , and R_s spectra is remarkably improved compared to the Lorentz approach of Figs. 2 and 3. In particular, the width and position of the plasmon resonance in the T spectrum are better described due to the sharper resonance of $\text{Im}\{\epsilon_{\text{DMY},//}\}$ compared to $\text{Im}\{\epsilon_{L,//}\}$. It can be noticed that the two components $\epsilon_{\text{DMY},//}$ and $\epsilon_{\text{MY},\perp}$ in Figs. 4(c) and 5(c) are of the same order as those in Figs. 2(c) and 3(c), the former show a different dispersion at short wavelengths which gives the correct spectral dependence of R_p , and R_s spectra. The latter feature is attributable to the onset of interband transitions in gold. These results indicate that the optical properties of these nanodisks arrays are dependent on their size, shape, properties of the constituent materials, and volume fraction.

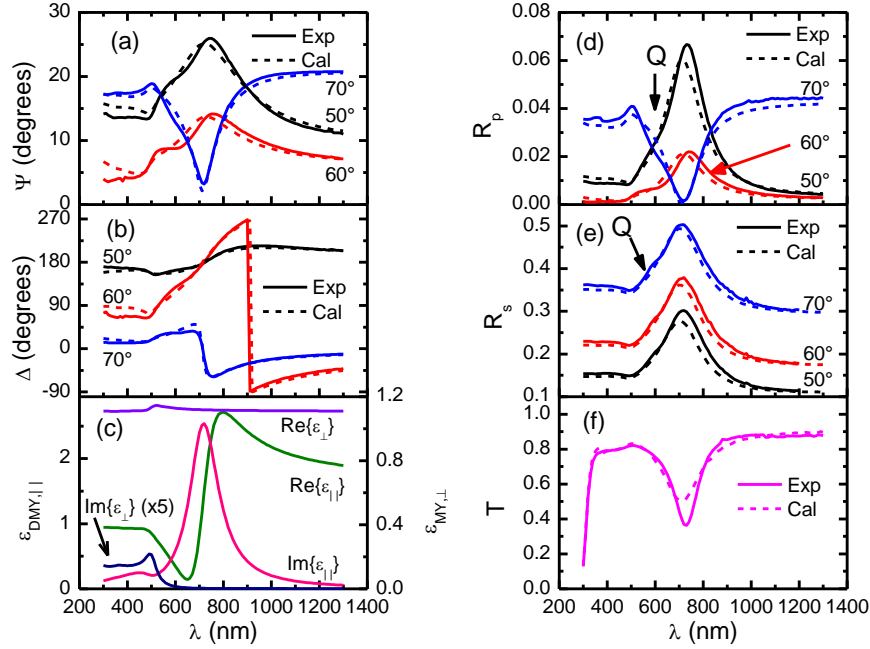


Fig. 5. Experimental and calculated spectra for a gold nanodisks array 40 nm thick using the dynamic Yamaguchi effective dielectric response assuming gold spheroids: (a) Ψ , (b) Δ , (c) effective dielectric function components, (d) reflectance of p-polarized and (e) s-polarized light, as well as (f) normal incidence transmittance.

3.3 Island film theory approach

Another formalism to be explored as a description of the optical response of the nanodisk arrays is the island-film theory. This theory is based on the concept of excess currents, charge densities and fields (\mathbf{E} , \mathbf{D} , \mathbf{B} , and \mathbf{H}) developed for the study of the optical properties of a film of islands attached to a flat substrate [27]. The island-substrate interface is assumed to be invariant with respect to translation, rotation and reflection in the x - y plane. In this theory, the film is replaced by a dividing surface somewhere within the film separating two homogeneous media, the ambient and the substrate. Then, excess polarization (\mathbf{P}^s) and magnetization (\mathbf{M}^s) densities are located at that dividing surface in such a way that the electromagnetic fields outside of the original film remain the same. Those excess quantities modify the boundary conditions and for non-magnetic systems in absence of spatial dispersion, the constitutive relations at the dividing surface are found to be: $\mathbf{P}_{||}^s = \gamma \mathbf{E}_{||,+}$, $\mathbf{P}_{\perp}^s = \beta \mathbf{D}_{\perp,+}$, and $\mathbf{M}^s = 0$, where the subscript “+” represents the average of the extrapolated values of the corresponding field at the dividing surface. The constitutive relations define the surface susceptibilities γ and β . Thus, for light incident from the ambient, modified Fresnel coefficients r_p and r_s are found and are given by [27,28],

$$r_s = \frac{n_a \cos \theta_i - n_s \cos \theta_t + i \left(\frac{2\pi}{\lambda} \right) \gamma}{n_a \cos \theta_i + n_s \cos \theta_t - i \left(\frac{2\pi}{\lambda} \right) \gamma}, \quad (8)$$

and,

$$r_p = \frac{\kappa_- - i \left(\frac{2\pi}{\lambda} \right) [\gamma \cos \theta_i \cos \theta_t - n_a n_s \varepsilon_a \beta \sin^2 \theta_i]}{\kappa_+ - i \left(\frac{2\pi}{\lambda} \right) [\gamma \cos \theta_i \cos \theta_t + n_a n_s \varepsilon_a \beta \sin^2 \theta_i]}, \quad (9)$$

where,

$$\kappa_{\pm} = (n_s \cos \theta_i \pm n_a \cos \theta_t) \left[1 - \frac{1}{4} \left(\frac{2\pi}{\lambda} \right)^2 \varepsilon_a \gamma \beta \sin^2 \theta_i \right]. \quad (10)$$

At normal incidence the transmission coefficient of the ambient-island film-substrate system can be calculated from [27,28],

$$t = \frac{2n_a}{n_a + n_s - i \left(\frac{2\pi}{\lambda} \right) \gamma}. \quad (11)$$

In Eqs. (8)–(11), $n_a (= \varepsilon_a^{1/2})$ and $n_s (= \varepsilon_s^{1/2})$ are the refractive indexes of the ambient and substrate, respectively; θ_i and θ_t are the incidence and refraction angles, respectively, related by Snell's law $n_a \sin \theta_i = n_s \sin \theta_t$. From Eqs. (8)–(11), the well known Fresnel coefficients for the ambient-substrate interface are obtained when $\gamma = \beta = 0$. The overall transmittance of light exiting from the back side of the substrate can be calculated according to,

$$T = |t_{sa} t|^2 \exp(-\alpha_s d_s), \quad (12)$$

where t_{sa} is to the transmission coefficient of the substrate-ambient back interface (this second reflection is neglected); α_s and d_s are the absorption coefficient and thickness of the substrate, respectively.

The next step requires the calculation of the two constitutive coefficients γ and β which for identical non-interacting particles (islands) are given by [27,28],

$$\begin{aligned} \gamma &= \rho \alpha_{\parallel}, \\ \beta &= \rho \alpha_{\perp} / \varepsilon_a^2, \end{aligned} \quad (13)$$

where ρ is the number of nanoparticles per unit area; α_{\parallel} and α_{\perp} are the in-plane and out-of-plane dipolar polarizabilities, respectively. These polarizabilities can be determined by multipole expansion of the potentials in the ambient and substrate and are expressed as a sum of the incident potential, the potential due to the charge distribution induced in the island, and the potential of the image charge distribution in the substrate. By applying the boundary conditions of those potentials at the surface of the substrate, an infinite set of linear equations for the expansion coefficients is obtained. In the practice, that set is numerically solved by neglecting multipoles larger than a suitable order. Also, analytical expressions for α_{\parallel} and α_{\perp} have been reported for spheres and spheroids (oblate and prolate). Herein, the nanodisks are represented as oblate spheroids and the polarizabilities in Eq. (13) can be obtained from the multipole expansion in spheroidal coordinates. In the dipolar approximation α_{\parallel} and α_{\perp} are given by [27],

$$\alpha_{\parallel, \perp} = \frac{4\pi a^2 c}{3} \frac{\varepsilon_a (\varepsilon_m - \varepsilon_a)}{[\varepsilon_a + L_{\parallel, \perp} (\varepsilon_m - \varepsilon_a)]}, \quad (14)$$

where a and c are the major and minor semi axes, respectively; ε_m is the nanodisks dielectric function; L_{\parallel} and L_{\perp} are the depolarization factors which for oblate spheroids touching the substrate are given by [27],

$$L_{\parallel} = l_{\parallel} + \frac{1}{2} (1 + e^2) \left(\frac{\varepsilon_a - \varepsilon_s}{\varepsilon_a + \varepsilon_s} \right) \left[e \arctan \frac{1}{e} - \left(e^2 + \frac{3}{2} \right) e^2 \ln \left(1 + \frac{1}{e^2} \right) + e^2 \right], \quad (15)$$

and,

$$L_{\perp} = l_{\perp} + (1 + e^2) \left(\frac{\varepsilon_a - \varepsilon_s}{\varepsilon_a + \varepsilon_s} \right) \left[e \arctan \frac{1}{e} - \left(e^2 + \frac{3}{2} \right) e^2 \ln \left(1 + \frac{1}{e} \right) + e^2 \right], \quad (16)$$

where $l_{(\parallel,\perp)}$ are the static depolarization factors and the nanodisks-substrate interaction is accounted through terms multiplied by the factor $(\varepsilon_a - \varepsilon_s)(\varepsilon_a + \varepsilon_s)^{-1}$ (<0 for an air-glass interface). It can be noticed that as a result of this interaction, $2L_{\parallel} + L_{\perp} \leq 1$. Also, the interaction with the substrate decreases the depolarization factors resulting in a shifted plasmon resonance to longer wavelengths.

This formalism has been used to analyze the optical response including the ellipsometric spectra of nanocolloidal gold particles on silicon [29], hexagonal arrays of silver nanocrystals on highly oriented pyrolytic graphite [30], and silver clusters supported on α -Al₂O₃ substrates [31]. In these works, the authors corrected the intraband contribution to the metal dielectric function (modifying the relaxation time in the Drude term) because the particle size was smaller than the bulk mean free path.

In the present case, the relative large diameter of the nanodisks makes it necessary to consider dynamic depolarization and radiation damping effects for the in-plane component α_{\parallel} which is renormalized according to [5,15,37],

$$\frac{1}{\alpha_{\parallel}^*} = \frac{1}{\alpha_{\parallel}} - \frac{k^2}{4\pi a} - i \frac{k^3}{6\pi}, \quad (17)$$

and in Eq. (13) α_{\parallel} should be substituted by α_{\parallel}^* . It can be noticed that in Eqs. (8)–(17) the input parameters are only the lengths of major and minor semi axes a and c , respectively, and the number of nanodisks per unit area ρ . The extinction spectra of supported metallic nanodisks have been analyzed with Eq. (17) but an averaged refractive index was used for the surrounding medium [14,15].

Figure 6 shows the calculated optical spectra with the island-film theory for the array of SiO₂ capped 20 nm thick gold nanodisks. The calculations were performed with a FORTRAN code with $a = 89$ nm, $c = 9$ nm, and $\rho = 4.5 \mu\text{m}^{-2}$. It can be noticed that the values of the semi axes a and c are comparable to the nominal radius (85 nm) and half thickness (10 nm), respectively. Also, the value of ρ is in agreement with the volume fraction q introduced in Sec. 3.2 because they are related by $q = \rho 4\pi a^2 c / 3d$. As can be seen in Fig. 6, the calculated spectra reproduce qualitatively and quantitatively all main features in the experimental data. The constitutive coefficients γ and β show a strong anisotropy of the in-plane and out-of-plane surface susceptibilities, Fig. 6(c). It can be noticed that both, the dynamic Yamaguchi (Fig. 4) and the island film theory (Fig. 6) approaches, give very similar optical spectra. However, the dynamic Yamaguchi effective medium approach is preferred because the spheroid parameters used, $a = 85$ nm and $c = 10$ nm, agree with the nominal radius and half thickness of the nanodisks.

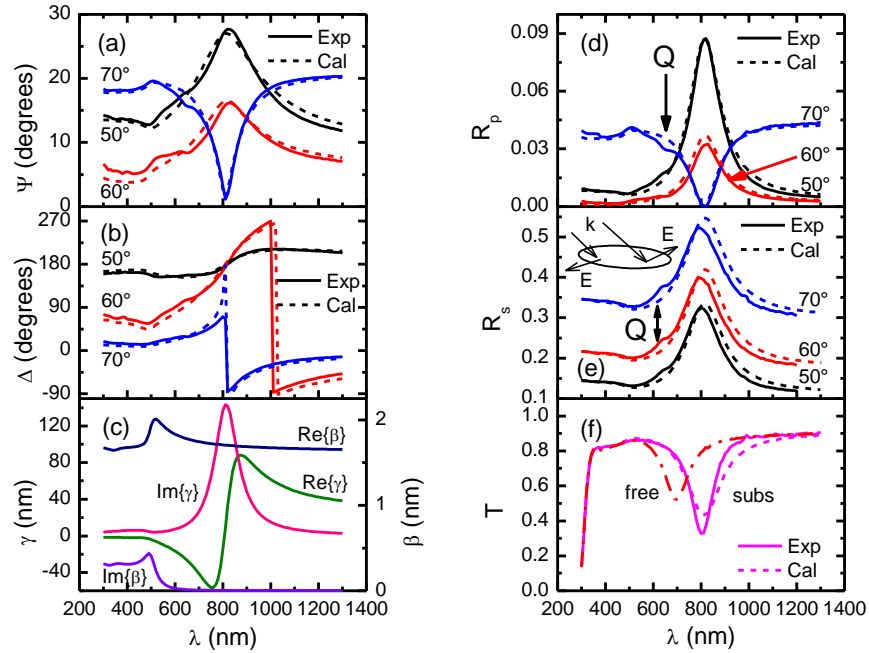


Fig. 6. Experimental and island-film theory calculated spectra for the silica-capped Au nanodisks array with thickness 20 nm: (a) Ψ , (b) Δ , (c) in-plane γ and out-of-plane β surface dipolar susceptibilities, (d) p-polarized reflectance, (e) s-polarized reflectance, and (f) normal incidence transmittance (subs). In (f) also the spectrum neglecting the spheroids-substrate interaction (free) is included.

3.4 In-plane anisotropy

Figure 7 shows the transmission ellipsometry data at normal incidence of the gold-silica nanostructured arrays. The measurements were performed at two different orientations, one from an arbitrary orientation (A) and the other by rotating the sample 90° to an orientation $A + 90^\circ$. In Fig. 7(a) around the plasmon resonance wavelength of 800 nm, Ψ shows small but significant deviations by less than $\pm 1^\circ$ from the isotropic case (45°) whereas in Fig. 7(b) the deviations in Δ from 0° are about $\pm 2^\circ$. These deviations indicate some in-plane anisotropy which exact origin is unknown at present. One possible explanation is by considering that the hole-mask colloidal lithography process produces “nearly” circular shaped nanodisks. In first approximation they can be represented as elliptical nanodisks with in-plane semi axes a and b (see the insert in Fig. 7(a)). Within this approximation, for incident light polarized parallel to a (b) the optical response can be described by an in-plane effective dielectric function $\epsilon_{\parallel,a}$ ($\epsilon_{\parallel,b}$). In the general case, when the nanodisks frame (a,b) is rotated by an angle ϕ with respect to the laboratory frame (p,s), the ratio of the transmission coefficients t_p and t_s in Eq. (1) for p and s polarizations depends on the averaged dielectric functions given by $\epsilon_p = \epsilon_{\parallel,a} \cos^2\phi + \epsilon_{\parallel,b} \sin^2\phi$ and $\epsilon_s = \epsilon_{\parallel,a} \sin^2\phi + \epsilon_{\parallel,b} \cos^2\phi$, respectively. Following the procedure described in Sec. 3.2, $\epsilon_{\parallel,a}$ and $\epsilon_{\parallel,b}$ for ellipsoidal particles will depend on the four terms considered in Eq. (6) as was done for spheroidal particles. In that case, the depolarization factors in the electrostatic limit l_a and l_b can be obtained from the integral form [1]. Nevertheless, the complete calculation of $\epsilon_{\parallel,a}$ and $\epsilon_{\parallel,b}$ is not possible because analytical expressions accounting for interaction with the substrate, dynamic depolarization, and radiation damping for ellipsoidal disks are not available. Another possible origin of the in-plane anisotropy could be due to the exact shape of the nanodisks. That is, depending on the procedure employed for fabrication of the nanodisks, either straight sidewalls or oblique truncation of the top as well as different nanoscopic roughness are obtained [11]. Furthermore, given the high sensitivity of

transmission ellipsometry (as compared with irradiance transmittance measurements), it could be employed to investigate a likely weak nanodisks interaction by varying the interparticle spacing and analyzing the effect on the in-plane anisotropy. However, such comprehensive study is beyond of the scope of this work.

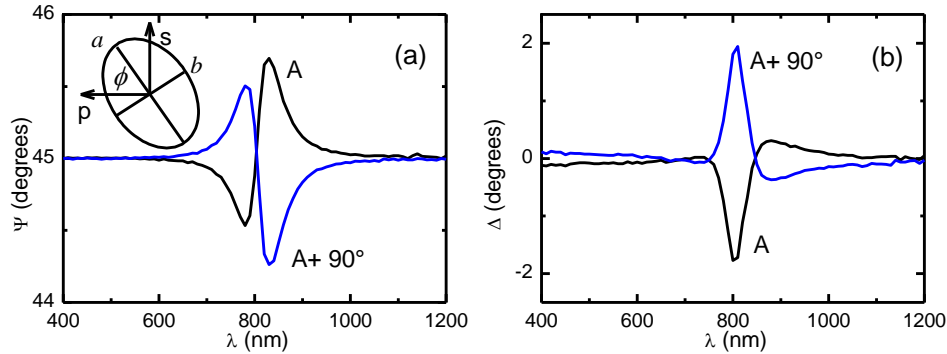


Fig. 7. Transmission ellipsometry spectra of Ψ (a) and Δ (b) at normal incidence for the silica capped Au nanodisks array 20 nm thick at two orientations differing by 90° . The insert in (a) shows an ellipsoidal nanodisk with semi axes (a,b) rotated an angle ϕ from the (p,s) frame.

3.5 Quadrupolar coupling

As discussed in Sec. 3.2 and 3.3, the main features in the experimental spectra can be quantitatively reproduced by modeling the nanodisks as oblate spheroids in the long-wavelength limit. However, both the 2D Yamaguchi model and the island-film theory are unable to reproduce the features of the R_s spectra and in the R_p (70°) spectrum at about 640 nm in Figs. 2, 4 and 6 and at 600 nm in Figs. 3 and 5. That is because their origin is a quadrupolar effect which cannot be included in the present models. At normal incidence the phase of the incident wave does not change across the diameter of the nanodisks which are homogeneously polarized and Eqs. (4) and (17) apply. On the other hand, increasing the angle of incidence there will be an appreciable phase difference of the incident wave on the two opposite extremes of the nanodisks, see the insert in Fig. 6(e). This phase retardation creates an inhomogeneous polarization field inside the nanodisks and quadrupolar moments can be coupled. It has been reported that for the extinction spectra measured at oblique incidence of 70° for s-polarized light transmittance, a second peak emerge at shorter wavelengths than the plasmon resonance in Au-nanodisks arrays 20 nm thick with diameter of 213 or 355 nm [39]. For the larger nanodisks arrays the quadrupolar resonance was imaged using apertureless scanning near-field optical microscopy [39]. These retarding effects in large particles coupling quadrupolar resonances have been reported using T-matrix calculations and finite-element modeling for silver spheroids and spheres, respectively [23,40]. By using the discrete dipole approximation, the optical spectra of isolated nanoparticles with different shapes have been studied and a richer spectrum was found for particles with sharp edges [41]. Also, the excitation of multipolar modes for small spheroids lying on a substrate has been studied using a spectral representation [42]. Surface difference reflectivity spectroscopy of small silver nanoparticles have shown that besides particle and substrate interactions multipolar effects arises due to the particle truncation when it is brought in contact with the substrate [43]. Therefore, the inhomogeneous incident field at larger angles of incidence and the sharp edges of the nanodisks real shape contribute to the quadrupolar feature. Finally, the results of this work will be valuable for a better understanding of the optical response of more complex nanostructures where nanodisks are the building blocks, for example as in nanosandwiches [9–11,44].

4. Conclusions

The effective optical response of gold-based nanostructured arrays produced by hole-mask colloidal lithography has been studied using two approaches. First, it was found that the ellipsometry spectra in the reflection mode can be described by modeling the nanostructured arrays as homogeneous uniaxial layers with dielectric functions of the Lorentz type. However, model-calculated spectra for oblique reflectance deviate from the experimental data at short wavelengths and the plasmon resonance is red-shifted and broader for normal incidence transmittance. Instead, modeling the nanodisks as oblate spheroids, the modified dynamic Yamaguchi effective medium expression qualitatively and quantitatively describes all measured spectra. The second approach considered was the island-film theory representing the nanodisks as oblate spheroids interacting with the substrate. Also, radiation damping and dynamic depolarization effects for the in-plane polarizability were considered. It was revealed that details of the nanostructured arrays are important to give a more complete description of all measured optical spectra. A small in-plane anisotropy detected by transmission ellipsometry spectra could be due to factors like deviation of circularity of the nanodisks, sidewalls shape, nanoscopic roughness as well as a weak nanodisks interaction. Furthermore, the complexity of the optical response increases because quadrupolar coupling arises at oblique incidence which cannot be included within the models here used.

Acknowledgments

AMG acknowledges the complementary support of Conacyt-Mexico with grant No. 80814 for spend a sabbatical leave at Linköping University and of the Fondo Sectorial de Investigación para la Educación grant No. 103385 to continue this work. Knut and Wallenberg Foundation is acknowledged for support to instrumentation.